3D seismic reflection data reveal syn-depositional halokinesis in the Zechstein Supergroup (Lopingian), Central North Sea, UK

Amir Joffe [1*], Christopher A-L. Jackson[2], Leonardo M. Pichel[3]

1. Basins Research Group (BRG), Department of Earth Science and Engineering, Imperial College London, South Kensington Campus, SW7 2BP, UK
2. Department of Earth and Environmental Sciences, The University of Manchester, Williamson Building, Oxford Road, Manchester, M13 9PL, UK
3. Department of Earth Science, University of Bergen, Allégaten 41, 5007, Bergen, Norway

Abstract

Salt tectonics is typically caused by the flow of mobile evaporites in response to *post-depositional* gravity gliding and/or differential loading by overburden sediments. This situation is considerably more complex near the margins of salt basins, where carbonate and clastic rocks may be deposited at the same time and interbedded with, more mobile, evaporite strata. In these cases, *syn-depositional* salt flow may occur due to density differences in the deposited lithologies, although our understanding of this process and related produces is relatively poor. We here use 3D seismic reflection and borehole data from the Devil's Hole Horst, West Central Shelf, offshore UK to understand the genesis, geometry and kinematic of intra-Zechstein Supergroup (Lopingian) minibasins and their effect on post-depositional salt deformation. Unlike much of the North Sea and other salt basins, the area is affected by only modest post-depositional, salt-related deformation, meaning it is a prime location to understand syn-depositional salt-related deformation. We show that intra-basin highs are dominated by immobile, pinnacle-to-barrier-like, carbonate build-ups and anhydrite, whereas mobile halite, which flowed to form large diapirs, dominates in the deep basin. At the transition between these two main domains, a belt of intra-Zechstein minibasins occur, forming due to the subsidence of relatively dense anhydrite into underlying halite. Depending on primary halite thickness, these intra-Zechstein minibasins created topographic lows, dictating the position for nucleation and subsequent down-building of Triassic minibasins. Our study refines the original depositional model for the Zechstein Supergroup in the Central North Sea, with the results also helping us better understand the style and distribution of syn-depositional salt flow in other layered evaporitic sequences and the role intra-salt heterogeneity and related deformation may have in the associated petroleum plays.

Introduction

Salt tectonics occurs in >100 sedimentary basins worldwide and is responsible for the formation of a remarkably complex range of structures (see Jackson and Hudec, 2017). These structures are important, given they can strongly influence the tectonostratigraphic evolution and petroleum system development of these basins. Most studies focus on the structural styles and stratigraphic patterns related to *post-depositional* salt flow; i.e. the post-depositional mobilization of the salt in response to differential sediment loading, gravity gliding and/or thick-skinned tectonics (Talbot and Jackson, 1987; Peel et al., 1996; Volozh et al., 2003; Hudec and Jackson, 2004; Brun and Mauduit, 2008, 2009; Quirk et al., 2012; Fernandez et al., 2017; Pichel et al., 2018; C.A.-L. Jackson, Duffy, et al., 2019). In this case, the timing and style of salt flow is typically recorded by deformation and stratigraphic patterns within the seismically well-imaged, supra-salt sedimentary sequences (Jackson and Hudec, 2017). Conversely, much less is known about the drivers and consequences of *syn-depositional* salt flow, for example how this relates to the primary lithology distribution within the layer, what types of intra-salt structural styles form because of this relatively early movement, or how syn-depositional movement impacts subsequent post-depositional salt flow and related deformation. Our lack of knowledge of these processes and products possibly reflects the fact that evidence for syn-depositional salt flow is often harder to obtain, given the difficulties associated with the seismic reflection imaging of the internal (i.e. intra-salt) structure and stratigraphy of subsurface salt bodies (see Jones and Davison, 2014). However, modern 3D seismic reflection data can occasionally image intra-salt layering and complex intra-salt deformation patterns (e.g. Central North Sea, offshore UK; Van Gent et al., 2011; Cartwright et al., 2012; Santos Basin, offshore Brazil; e.g. Gamboa et al., 2008; Davison et al., 2012; Fiduk and Rowan, 2012; Dooley et al, 2015; Jackson et al., 2015; Pichel et al., 2019; the Levant Basin; e.g. Gvirtzman et al., 2013). In some of these examples, the relative timing between salt deposition and deformations is debatable, principally due to intense post-depositional salt flow and diapirism obscuring the evidence of early-formed intra-salt structures and stratigraphic patterns (i.e. thickness changes, onlaps) (Gamboa et al., 2008; Davison et al., 2012; Fiduk and Rowan, 2012; Dooley et al., 2015).

In the Central North Sea, offshore eastern UK, syn-depositional salt flow has been described in the Zechstein Supergroup (Clark et al., 1998) (Figure 1). These authors show several 2D seismic profiles characterising the seismic expression and structural style of intra-Zechstein, syn-depositional minibasins, which they refer to as 'rafts'. Using vintage 3D seismic reflection data they produce a series of thickness maps to illustrate how a single intra-salt minibasin evolved, showing that the depocenter location was not fixed, but instead shifted through time (Figure 1C, 1D). How this behaviour related to the growth of adjacent salt structures and subsidence patterns in nearby minibasins was not discussed.

We here expand on the ideas initially formulated by Clark et al. (1998) by using modern, 3D seismic reflection and borehole data from the eastern flank of the Devil's Hole Horst, UK Central North Sea (Figure 1A). The study areas lie in a location characterised by marked spatial changes in the lithology and overall thickness of the Zechstein Supergroup. The study area, coupled with minimal post-depositional deformation and high-resolution seismic imaging make the southern corner of the Devil's Hole Horst a prime location to revisit this key salt-tectonic problem (Figure 1A). By integrating 3D seismic reflection data and well data, we can: (1) characterize and map syn-depositional, salt-related deformation within the Zechstein Supergroup; (2) relate the structural style of syn-depositional minibasins to primary lithology variations within the salt; and (3) explore how the syn-depositional salt flow influenced post-depositional salt and overburden deformation.

Geological Setting

The main tectonic event that influenced the location and extent of the evaporites of the Zechstein Supergroup was Cisuralian (Early Permian) rifting associated with the development of the Central Graben (e.g. Ziegler, 1975; Hodgson et al., 1992). During the early stages of rifting, subsidence rates exceeded sediment accumulation rate, forming a sediment starved, intra-continental basin (Hodgson et al., 1992; Penge et al., 1993; Smith et al., 1993). A marine transgression during the Guadalupian (Middle Permian) resulted in desert lakes filling the rift-related relief, which when coupled with limited influx of marine seawater, enabled the development of hyper-saline conditions and the deposition of an evaporite-bearing sedimentary sequences (Hodgson et al., 1992; Penge et al., 1993; Smith et al., 1993). More specifically, 4-5 cycles of flooding and evaporation during the Lopingian (Late Permian) resulted in the deposition of a layered evaporitic sequence known as the Zechstein Supergroup (Smith et al., 1993; Armour et al., 2004). Repeated flooding and evaporation directly influenced lithology distribution in the Zechstein Supergroup, i.e., carbonate- and anhydrite-rich units were deposited at the basin margins and on intra-basin structural highs during highstands, whereas halite- and K-Mg-rich salt-rich units were deposited in the deeper basins during lowstands (Tucker, 1991).

Based on the percentage of halite found in boreholes and inferred from salt-related structural styles imaged in seismic reflection data, the Zechstein Supergroup is divided into four depositional zones (DZ) (Figure 1A, 1B). DZ1 is located along the basin margins on intra-basin structural highs, and consists mainly of shelfal carbonate, anhydrite, and clastic rocks, with little or no halite (<10%). DZ2 is similar to DZ1 but contains a higher percentage of halite (10-50%), whereas DZ3 is characterized by relatively minor amounts of shallow waters shelfal rocks and a larger proportion of halite (50-80%). DZ2 and DZ3 together define the transition from the basin margin to basin centre, and they were typically deposited on and thus define, basinward-dipping slopes (Clark et al., 1998; Patruno et al., 2018; Grant et al., 2019; C.A.-L. Jackson, Elliott, et al., 2019). 3D seismic-based analysis of the Mid-North Sea High by Patruno et al. (2018) indicate that this transitional region may be composed of a hybrid sulphate-carbonate platform (Z1-2; Taylor, 1998), capped by a thin, Z3-dominated carbonate platform (Z3; Taylor, 1998). Using the terminology of Clark et al. (1998), we would therefore assign the Mid-North Sea High region to DZ1 or 2. Finally, the deep basinal areas are defined by DZ4, which consists almost entirely of halite (>80%). In this zone diapirs and deep minibasins represent the main salt-tectonic structures; in contrast, DZ1 and 2 are largely undeformed or only weakly deformed due to the lack of mobile salt (Clark et al., 1998; C.A.-L. Jackson, Elliott, et al., 2019).

A second pulse of rifting during the Early Triassic reactivated the basement-involved, sub-salt faults, triggering post-depositional flow and reactive rise of the overlying Zechstein Supergroup salt. In the halite-rich DZ3 and DZ4, stocks and N-trending salt walls formed. Triassic salt tectonics resulted in relatively thick sequences of nonmarine Triassic rocks being contained within minibasins; these sequences thin towards and onlap flanking salt bodies (Figure 2) (Ziegler, 1975).

Data and Workflow

We use a 6,580 km^2 pre-stack time-migrated 3D seismic volume, that covers Zechstein Supergroup DZ2- DZ4 (Figure 1). The dataset is in the NE portion of Quadrant 28 on the United Kingdom Continental Shelf (UKCS), adjacent to areas in which Clark et al. (1998) documented the syn-depositional flow and deformation of Zechstein Supergroup salt (Figure 1A). Six wells were also available for this study; two wells are in DZ3 (28/9-4 & 28/4a) and four in DZ4. In our dataset, the lithology of DZ1 and DZ2 are not constrained by wells and must thus be inferred from the prevailing salt-related structural style (see Clark et al., 1998; Jackson et al., 2019). Two wells (28/4a-2 & 28/5-1) are only c. 10 km apart, allowing us to constrain the boundary between DZ3 and DZ4 with relative precision (Figure 1A).

Well-log data from wells were used to directly determine lithological variations within the Zechstein Supergroup. Well data also constrained the age of four regional seismic reflections (base and top Zechstein, top Triassic, Top Jurassic), and one intra-salt reflection, which we mapped across the dataset. The base and top Zechstein Supergroup reflections define the key salt-bearing interval, whereas the locally mappable intra-salt reflection separates weakly reflective, halite-rich sequences below from more reflective, halite-poor sequences above (see below). This distinction becomes important later when discussing seismic-stratigraphic evidence for syn-depositional salt flow. Triassic minibasins, capped by the top Triassic reflection, are very weakly reflective, whereas the overlying Jurassic interval, bound below and above by the top Triassic and top Jurassic, respectively, is very reflective (Figure 2).

Results

Composition and Seismic Expression of the Zechstein Supergroup

We determined the composition of the Zechstein Supergroup using well-log data. Two wells (28/4a-2 & 28/5-1) penetrated and logged the entirety of the Zechstein Supergroup, whereas the other four penetrated and logged only its upper portion. The former two wells prove a 30-

50 m thick carbonate layer at the base of the otherwise evaporite-rich sequence (Figure 2). This basal carbonate-rich unit characterises the Zechstein Supergroup across much of the North Sea, recording the temporal transition from the non-marine environment recorded by the Rotliegend Group to the more restrictive marine conditions in which the Zechstein was deposited (Glennie and Underhill, 1998; Brackenridge et al., 2020). Well 28/5-1, which penetrates a diapir in DZ4 (c. 90% halite), shows an abrupt upward transition from the carbonate layer into a thick (650 m) halite interval, whereas the basal carbonate in well 28/4a-2 is separated from the overlying halite unit (c. 60% of the total penetrated thickness) by a thin (c. 25 m), claystone-bearing unit. In all wells the Zechstein Supergroup is capped by a 25-90 m thick anhydrite-dominated unit that is locally interbedded with thin (5-10 m) layers of claystone (Figure 2). Based on its occurrence at the top of areas of inflated salt (i.e., diapirs), we infer that this unit represents crestal caprock, formed by the preferential dissolution of halite and other soluble rock types like potash salts (e.g. Ulrich et al., 1984; Warren, 2006). Halite dominates the core of the underlying diapirs, as proven by 28/5-1 and 28/4a-2.

Zechstein Supergroup Structural Framework

The base Zechstein surface has a convex-to-the-basin plan-view geometry that broadly dips eastwards (Fig. 3A). This convex shape reflects the study area’s location on the eastern flank of Devil’s Hole Horst (Figure 1A). We also note that this shape mimics the boundaries between the depositional zones mapped by Clark et al. (1998) (Figure 1A). The base Zechstein surface is relatively smooth, although an E-W striking, N-dipping fault occurs in the north-eastern part of the dataset (Figure 3A).

In a similar manner to the base Zechstein surface, the top Zechstein surface also dips eastwards. The surface is, however, not smooth, but instead defines numerous salt diapirs, the most prominent of which are defined by three broadly curvilinear, sub-parallel, convex-into-the-basin salt walls (SW1-SW3; Figure 4A). These walls are 1.5-7 km wide, 150-500 ms tall, and at least 30 km long, extending northwards and southwards outside of the dataset. SW1 and SW2 have very well-defined, smooth margins but SW3 is more amorphous, being characterized by several W-trending, spur-like walls that protrude from its eastern margin (Figure 4A). We observe shorter protrusions, with a similar easterly trend, along the eastern edge of SW2. The salt walls are separated by minibasins that are, between SW2 and SW3, broadly N-trending, elongate, and convex-into-the-basin, like their bounding diapirs (MB2) (Figure 4A). The minibasin between SW1 and 2 (MB1) dies-out north-eastwards as the flanking salt walls merge to form a broader salt plateau (minibasin 1; Figure 4A, 5). MB2 and other minibasins in the southerly portion of SW3 contain isolated salt stocks that are 0.4-1.5 km in diameter and up to 500 ms tall (Figures 4B, 6).

Intra-Zechstein Structures

Intra-Zechstein Seismic Facies

Two key seismic facies are present in the Zechstein Supergroup. The first is a chaotic unit that is prominent at the base of the Zechstein Supergroup and which defines the core of the most prominent salt structures, such as diapirs (Figures 5, 6). The second is a more reflective, well-layered unit that occurs almost exclusively in upper part of the Zechstein Supergroup, and which typically occurs in broadly bowl-shaped packages that thin towards and onlap onto flanking diapirs (Figure 5 - 9). The latter is restricted to the SE of the study area, mostly within DZ3 as mapped by Clark et al. (1998) (Figure 1, 3D, 3E).

We interpret that the intra-salt reflectively and seismic facies changes in the Zechstein Supergroup marks an upward transition from a halite-rich, diapiric unit (proven by wells 28/5-1 and 28/4a-2; Fig. 2; cf., Jackson et al., 2015) to a more heterogeneous, anhydrite-dominated unit (c.f. Rodriguez et al., 2018). Based on its bowl-shaped external form, and the fact that internal reflections thin towards and onlap onto structures composed of the more chaotic seismic facies, we interpret that intra-salt reflectivity in the upper part of the Zechstein

Supergroup define intra-salt minibasins, similar to those interpreted elsewhere in the Central North Sea (Clark et al., 1998; Jackson and Stewart, 2017). These intra-Zechstein minibasins are thinnest along the westerly part of the study-area and within MB1, and thicker to the southeast (Fig. 3C). We also note that these minibasins may be perched along the flanks of the diapiric salt walls and, occasionally, encased within the walls themselves (Figure 3E).

Intra-Zechstein Structural Framework

To better understand the types and possible origins of the different styles of intra-Zechstein minibasins, we provide four examples of their structural and stratigraphic context using four cross-sections trending broadly east, parallel to the structural dip of the base Zechstein (Figure 3D).

<u>Section 1</u>

The first cross-section is located within DZ2 and DZ3 and reveals several broadly mounded structures at the base of the Zechstein (Figure 7A, 7D). These structures are capped by a distinct high-amplitude positive (red) reflection that continuous westwards, towards the basin margin. The mounds form a series of approximately NNW-trending, 200-300 m-wide, up to 200 ms-tall, crescentic features (south of Figure 7C), or lower-relief, more amorphous features (north of Figure 7C). These mounds are overlain by the two key seismic facies described above (i.e., halite-rich diapiric salt; deep pink in Figure 7B and an anhydrite-rich minibasin; light-pink in Figure 7B). The latter locally onlaps the largest mounded structure at the base of the Zechstein Supergroup (Figure 7B). Here, a third seismic facies is observed locally at the top of the Zechstein Supergroup; this is defined by moderate- to high-amplitude reflections that onlap onto and dip away from diapiric highs (Figure 7B).

Based on their mounded geometry and seismic expression (Figure 7D), the abundance of carbonates at the base of the Zechstein Supergroup as shown by the wells (Fig. 2), and their tectono-stratigraphic context at the evaporitic basin margin , we interpret these base-Zechstein features as carbonate build-ups (Figure 7B, 7D). These features are in an area previously identified by Clark et al. (1998) as being carbonate-rich, further supporting our interpretation. Similar carbonate-related features are documented in the Southern North Sea (Grant et al., 2019). East of the largest mound, a minibasin separates the domain of base-Zechstein carbonate build-ups from a halite-rich salt wall; the minibasin onlaps both flanking structures (Figure 7B).

Section 2

The second cross-section is located mostly within DZ3. The most prominent features in this section are the large, halite-rich diapirs (Figure 8). Small (150 ms tall by 1000 m wide), triangular-shaped and generally more reflective bodies also occur locally at the base of the Zechstein Supergroup. These bodies are onlapped and/or downlapped by highly reflective, sigmoidal, clinoform-like reflections (Figure 8). These highly reflective sigmoidal reflections are thickest adjacent to the large diapir to the east, onlapping its western flanks, forming an asymmetric minibasin that is welded to the sub-salt strata (Figure 8B). The overlying Triassic is broadly isopachous, indicating that most of the mobile halite-dominated package below was evacuated before the its deposition (Figure 8B). Where present, minor thickness variations in the Triassic minibasin mirror the thickness variation in the intra-Zechstein packages. We identify another relatively small (200 ms thick), intra-salt minibasin in the centre of the cross-section (Figure 8A).

Section 3

The third cross-section shows two relatively thin (200-250 ms), bowl-shaped packages of continuous, intra-Zechstein reflections perched within a large salt wall (SW3; Figure 9A). These packages thin towards and onlap onto flanking diapirs (Figure 9A). A similar, albeit highly asymmetric sequence is also present dipping eastwards on the eastern flank of the large wall and being overlain and indented by a small, Triassic minibasin (Figure 9A). Across the section, Jurassic strata are broadly tabular and generally sub-horizontal, locally thinning across and onlapping onto Triassic minibasins where these protrude above the top salt (Figure 9). We suggest that the easterly dips within the easternmost intra-Zechstein minibasin was caused by the subsequent subsidence of Triassic clastic strata down into the salt, which caused tilting of previous deposited evaporitic rocks (Figure 9B).

Section 4

Unlike the previous examples, the fourth and final example is located in the southern-easterly part of the dataset (Figure 3D). This area is characterised by higher density of intra-Zechstein minibasins, and higher structural complexity (Figure 3C). In this example, two Triassic minibasins are present (MB1 and MB2) and separated by two salt walls (SW2 and SW3) (Figure 5). The broad bowl-shaped intra-Zechstein sequence below MB1 is relatively thin (150 ms), symmetrical cross-section (Figure 5) and elongate in map-view (Figure 4A). The intra-Zechstein minibasin below MB2 is thickest on the flanks of SW3, thinning both towards the crest of the diapir and updip towards the base of SW2. The Triassic minibasin MB2 is thickest where the intra-Zechstein minibasin onlaps SW2 (Figure 5).

Based on thickness relationships between intra-Zechstein and Triassic minibasins, we interpret that the post-Zechstein subsidence of Triassic minibasins into underlying salt caused the intra-Zechstein minibasins to rotate north-westwards (Figure 5B). We generally observe more complex deformation in the SE of the study area. In special, we see more evidence of tilting of intra-Zechstein minibasins due to the subsidence of younger, Triassic minibasins. The reason for this is not clear, but it might reflect the fact that in this region, down-flank of the Devil's Horse Horst, mobile halite was thicker and, therefore, there was still material to be evacuated from below the intra-Zechstein minibasins when Triassic minibasins formed.

Triassic

Triassic minibasins are characterized by weakly continuous, largely transparent seismic facies overlying the more reflective Zechstein Supergroup units (Figure 5, 6, 8). The relatively smooth (compared to the top-salt), regionally consistent eastward dip observed at the top Triassic level (Figure 4E) indicate that salt-related deformation peaked during the Lopingian-Early Triassic and declined during the Late Triassic-Early Jurassic. Top Triassic rugosity probably relates to dissolution of the crests of intervening salt diapirs and/or post-Triassic extension (Mannie et al., 2014).

Discussion

Syn-depositional salt-related deformation and controls on subsequent structural style

Using 3D seismic reflection and well data from the eastern flank of the Devil's Hole Horst, UKCS, we argue that although the Zechstein Supergroup depositional model of Clark et al. (1998) accurately captures the basin-scale distribution of the key rock types, because of its more regional focus, and the data quality and quantity at that time, it does not demonstrate how the variable density and mechanical properties of these rocks controlled syn- and post-depositional salt flow and related deformation. We have shown that intra-Zechstein salt flow was initiated before the deposition of Triassic overburden and was characterized by development of anhydrite-rich minibasins and halite-rich diapirs adjacent to and/or overlying basal carbonate build-ups. These results in lateral variability of intra-Zechstein lithologies and geometries influenced the subsequent Triassic deposition and architecture.

We thus propose an update to the idealized model of Clark et al. (1998), by incorporating both the structural and lithological variability observed within the Zechstein Supergroup in our study-area (Figure 10). Our model envisages the same four main Zechstein Supergroup depositional cycles and zones defined by Clark et al. (1998), with each cycle and zones consisting of initial carbonate deposition associated with marine transgression and basin flooding, followed by anhydrite, and then halite deposition during basin desiccation.

Deposition during the first cycle occurs across the generally smooth, basinward-dipping, base-salt surface. During this time, there is no gravitational potential or significant enough vertical density variations to drive salt flow and related deformation (Figure 10A). The second cycle starts with deposition of relatively dense carbonate at the basin margin, on top of less dense halite (Figure 10A). The deposition of dense carbonates and subsequent anhydrite on top of less dense and more mobile halite triggers down-dip salt evacuation, inflation, and diapirism of the latter (Figure 10B). The second cycle ends with the deposition of a second halite unit, coevally to the downdip flow, inflation and diapirism of the previous halite unit (Figure 10C). The third cycle is also characterised by the deposition of a basin-margin, carbonate-dominated unit (Figure 10D). Assuming the basinward flow of halite during the preceding phases was sufficient to generate a local, salt-cored structural high, the near-margin area may have been sufficiently shallow to allow the nucleation of shallow-water carbonates (Figure 10D). This element of the model is supported by the first example seen at Figure 7, which suggest that locally at least, carbonate build-ups could form on areas of inflated, halite-rich salt, at some distance into the basin. The third cycle continues with deposition of anhydrite (Figure 10E) followed by halite (Figure 10F). During deposition of these evaporitic cycles, mobile halite deposited during previous cycles continuous to flow down-dip due to loading at the basin-margin by dense, carbonate-/anhydrite-rich units (Figure 10E, 10F). By the fourth cycle (Figure 10G), a progradational carbonate platform developed along the basin margin, as observed in Figure 5, passing laterally basinward into anhydrite-rich minibasins surrounded by halite-rich salt walls.

The variability of halite proportion in each cycle governs the magnitude and location of salt-related deformation during Zechstein Supergroup deposition. The final halite thickness and proportion in each cycle also influenced the style and intensity of post-depositional (i.e. post-Lopingian) salt-related deformation (Figure 10H). In areas where the salt was halite-rich and relatively thick, post-depositional salt flow was substantial, allowing large diapirs to form; in contrast, in areas where mobile halite was relatively thin and impure, post-depositional deformation were less pronounced (Figure 3E). These differences in the magnitude of deformation governed by the amount and proportion of halite in the different cycles, are seen in our dataset, being expressed by the differences between the four cross-sections (Figures 7-9). For example, carbonate deposition at the basin margin promoted the syn-depositional basinward expulsion of mobile evaporites, favouring the development of larger Triassic minibasin above the anhydrite-dominated intra-Zechstein minibasins, lateral to the mechanically stronger carbonates (e.g., Figure 7). We also note that thickness changes in the Triassic minibasin mirror those in the intra-Zechstein, suggesting that subtle topographic lows above intra-Zechstein minibasins localised earliest Triassic deposition, thus triggering the nucleation and dictating the position of the Triassic minibasins (e.g., Figure 8). Conversely, where intra-Zechstein minibasins were small relative to their flanking salt walls, they did not act as nucleation sites for subsequent Triassic minibasins (e.g., Figure 9). Finally, we show that thicker (and generally larger) intra-Zechstein minibasins are preferentially formed where the mobile halite was initially thicker, in the deep basin (e.g., Figure 5).

In addition to being genetically related to the intra-Zechstein minibasins, the subsidence history of the Triassic minibasins may have been controlled by the older structures. For example, the Triassic minibasins contain strata units that are wedge- rather than bowl-shaped, which we infer document minibasin tilting during subsidence (Rowan and Weimer, 1998; C.A.-L. Jackson, Duffy, et al., 2019). The reason for this is not clear, but it may reflect the fact that

Triassic minibasins impinged on the underlying Zechstein minibasin as they subsided, with the latter containing relatively rigid, largely immobile anhydrite flanked by more mobile halite. Such similar interactions between intra-salt and supra-salt was observed in the Precaspian Basin (Fernandez et al., 2017), where encased intra-salt minibasins dip towards the supra-salt minibasins as a consequent of loading by the younger minibasin strata (see Figures 12 and 15 in their text). As such, our conceptual model may be more broadly applicable to other basin-margin and intra-basin high positions in the Zechstein salt basin, as well as comparable locations in other global salt basin containing layered evaporite sequences (see below).

Implications for understanding salt tectonics and petroleum systems in other salt basins

Although based on an analysis of the Lopingian salt in the North Sea, the results of our study may have more general, broader implications for understanding to salt tectonics and related petroleum systems development in other salt basins. In the Precaspian Basin, numerous, very large (up to 3 km thick), Permo-Triassic, intra-salt minibasins are encased in thick, Kungurian (Lower Permian) salt. Well data indicate that these intra-salt basins contain mix of clastic, carbonate, and evaporite (i.e., halite, anhydrite) rocks (Fernandez et al., 2017). The authors suggest that the large proportion of relatively dense anhydrite and carbonate within these minibasins was a key reason for their relatively quick encasement, confirming the importance of vertical (i.e., stratigraphic) lithology and density variations in driving syn-depositional salt flow and tectonics. Lateral (i.e., areal) variations in lithology and thus density likely also play a key role in determining when and where sun-depositional salt flow and tectonics, and when minibasin encasement might occur. For example, in the North Sea and Precaspian Basin, relatively early (i.e. syn-depositional) salt flow and tectonics occur towards the basin margin, where halite-rich and poor sequences are more likely to interfinger (see Tucker, 1991). Further basinward, halite dominated and insufficient anhydrite and/or carbonate are deposited to drive early subsidence; further landward and there is insufficient halite to flow and produce diapirs and minibasins.

A key question is, therefore, “how do we distinguish structural styles and thickness changes related to the relatively early, syn-depositional deformation of salt from those related to the relatively late, post-depositional flow of salt, in which case these changes may be simply strain induced?” (see Allen et al., 2016). Clearly, geological context and supporting data are critical. For example, is the study area located in a near-margin position where interbedded halite and denser, non-halite lithologies occur, and can be proven by wells or reasonable inferred from the overall basin settings? Does seismic-stratigraphic architecture and thickness changes in the inferred syn-kinematic sequences mirror those in the demonstrably younger, more obvious, salt-related packages, i.e., does the former occur in well-defined, bowl-shaped packages that thin towards and onlap onto flanking salt structures inferred or demonstrated to be halite-rich?

Syn-depositional salt tectonics clearly has important implications for petroleum systems development in salt basins. For example, intra-salt minibasins may contain carbonate and clastic reservoirs, capped and sealed by, and onlapping onto, impermeable halite, resulting in structural (or comminated structural-stratigraphic) traps similar to those developed in the Gulf of Mexico (e.g. Booth et al., 2003). Intra-salt minibasin, if they subside all the way through the underlying, halite-rich salt, may form turtle structures, forming 4-way dip closures (Jackson and Hudec, 2017). Welding may then provide these intra-salt minibasins to charge by otherwise inaccessible, sub-salt source rocks.

Conclusion

We used modern 3D seismic reflection and borehole data from the eastern flank of the Devil’s Hole Horst, UK Central North Sea to map and characterise syn-depositional salt related deformation within the Zechstein Supergroup. We show four examples of intra-salt minibasins, characterised by different lithological variations and/or structural styles and discuss their influence on syn-depositional salt flow and subsequent, post-depositional deformation. Our first example shows how intra-Zechstein minibasins and halite-dominated diapirs develop away from the mechanically stronger, carbonate-dominated Zechstein rocks. We then showed how subtle topographic lows created by the intra-Zechstein minibasin control the nucleation of post-depositional Triassic minibasins. Finally, we demonstrate that in places where halite was still thick after the end of salt-deposition due to either (i) syn-depositional mobilization/inflation or (ii) halite-rich deposition towards the deep-basin, post-depositional minibasins were highly asymmetric. By integrating these observations, we propose a revised and, in our view, improved kinematic-depositional model that correlates intra-Zechstein lithological variability with syn-depositional salt deformation. We thus believe that our model is more broadly applicable to other areas of the Zechstein salt basin than the one originally proposed by Clark et al. 1998. Our model can be also more applicable to worldwide layered evaporite sequences and may suggest that syn-depositional deformation is likely a more common phenomenon than often observed in areas affected by intense and long-lived post-depositional salt tectonics such as the Gulf of Mexico and South Atlantic. The results of this work have implications for hydrocarbon exploration and CO_2 sequestration in other salt basins, highlighting the structural and stratigraphic complexity which may occur in sequences classically considered only as seals.

Acknowledgments

We would like to acknowledge TGS for permission to use the seismic reflection data shown in this study, in particular Annette Flethøj Tvedten and Will King.

References

Allen, H., C. A.-L. Jackson, and A. J. Fraser, 2016, Gravity-driven deformation of a youthful saline giant: the interplay between gliding and spreading in the Messinian basins of the

Eastern Mediterranean: Petroleum Geoscience, v. 22, no. 4, p. 340–356, doi:10.1144/petgeo2016-034.

Armour, A., D. Evans, and C. Hickey, 2004, The Millennium A t l a s : petroleum geology of the central and northern North S e a THE MILLENNIUM ATLAS : of the CENTRAL and The project to produce the Millennium Atlas was organised by : Petroleum Geology.

Booth, J. R., M. C. Dean, A. E. DuVernay, and M. J. Styzen, 2003, Paleo-bathymetric controls on the stratigraphic architecture and reservoir development of confined fans in the Auger Basin: central Gulf of Mexico slope: Marine and Petroleum Geology, v. 20, no. 6, p. 563–586, doi:https://doi.org/10.1016/j.marpetgeo.2003.03.008.

Brackenridge, R. E., J. R. Underhill, R. Jamieson, and A. Bell, 2020, Structural and stratigraphic evolution of the Mid North Sea High region of the UK Continental Shelf: Petroleum Geoscience, v. 26, no. 2, p. 154–173, doi:10.1144/petgeo2019-076.

Brun, J. P., and T. P. O. Mauduit, 2008, Rollovers in salt tectonics: The inadequacy of the listric fault model: Tectonophysics, v. 457, no. 1–2, p. 1–11, doi:10.1016/j.tecto.2007.11.038.

Brun, J. P., and T. P. O. Mauduit, 2009, Salt rollers: Structure and kinematics from analogue modelling: Marine and Petroleum Geology, v. 26, no. 2, p. 249–258, doi:10.1016/j.marpetgeo.2008.02.002.

Clark, J. A., S. A. Stewart, and J. A. Cartwright, 1998, Evolution of the NW margin of the North Permian Basin, UK North Sea: Journal of the Geological Society, v. 155, no. 4, p. 663, doi:10.1144/gsjgs.155.4.0663.

Davison, I., L. Anderson, and P. Nuttall, 2012, Salt deposition, loading and gravity drainage in the Campos and Santos salt basins: Geological Society, London, Special Publications, v. 363, no. 1, p. 159 LP – 174, doi:10.1144/SP363.8.

Dooley, T. P., M. P. A. Jackson, C. A. L. Jackson, M. R. Hudec, and C. R. Rodriguez, 2015, Enigmatic structures within salt walls of the Santos Basin-Part 2: Mechanical explanation from physical modelling: Journal of Structural Geology, v. 75, p. 163–187, doi:10.1016/j.jsg.2015.01.009.

Fernandez, N., O. B. Duffy, M. R. Hudec, M. P. A. Jackson, G. Burg, C. A. L. Jackson, and T. P. Dooley, 2017, The origin of salt-encased sediment packages: Observations from the SE Precaspian Basin (Kazakhstan): Journal of Structural Geology, v. 97, p. 237–256, doi:10.1016/j.jsg.2017.01.008.

Fiduk, J. C., and M. G. Rowan, 2012, Analysis of folding and deformation within layered evaporites in blocks BM-S-8 & -9, Santos Basin, Brazil: Geological Society Special Publication, v. 363, no. 1, p. 471–487, doi:10.1144/SP363.22.

Gamboa, L. A. P., M. A. P. Machado, D. P. Da Silveira, J. T. R. De Freitas, S. R. P. Da Silva, W. Mohriak, P. Szatmari, and S. ANJOS, 2008, Evaporitos estratificados no Atlântico Sul: interpretação sísmica e controle tectono-estratigráfico na Bacia de Santos: Sal: Geologia e Tectônica, Exemplos nas Basicas Brasileiras, p. 340–359.

Glennie, K. W., and J. R. Underhill, 1998, Origin, Development and Evolution of Structural Styles: Wiley Online Books, p. 42–84, doi:https://doi.org/10.1002/9781444313413.ch2.

Grant, R. J., J. R. Underhill, J. Hernández-Casado, S. M. Barker, and R. J. Jamieson, 2019, Upper Permian Zechstein Supergroup carbonate-evaporite platform palaeomorphology in the UK Southern North Sea: Marine and Petroleum Geology, v. 100, p. 484–518, doi:10.1016/j.marpetgeo.2017.11.029.

Hodgson, N. A., J. Farnsworth, and A. J. Fraser, 1992, Salt-related tectonics, sedimentation and hydrocarbon plays in the Central Graben, North Sea, UKCS: Geological Society, London, Special Publications, v. 67, no. 1, p. 31 LP – 63, doi:10.1144/GSL.SP.1992.067.01.03.

Hudec, M. R., and M. P. A. Jackson, 2004, Regional restoration across the Kwanza Basin, Angola: Salt tectonics triggered by repeated uplift of a metastable passive margin: AAPG Bulletin, v, v. 88, no. 7, p. 971–990, doi:10.1306/02050403061.

Jackson, C. A.-L., O. B. Duffy, N. Fernandez, T. P. Dooley, M. R. Hudec, M. P. A. Jackson, and G. Burg, 2019, The stratigraphic record of minibasin subsidence, Precaspian Basin, Kazakhstan: Basin Research, v. 0, no. 0, p. 1–25, doi:10.1111/bre.12393.

Jackson, C. A.-L., G. M. Elliott, E. Royce-Rogers, R. L. Gawthorpe, and T. E. Aas, 2019, Salt thickness and composition influence rift structural style, northern North Sea, offshore Norway: Basin Research, v. 31, no. 3, p. 514–538, doi:10.1111/bre.12332.

Jackson, M. P. A., and M. R. Hudec (eds.), 2017, Salt Tectonics, *in* Salt Tectonics: Principles and Practice: Cambridge, Cambridge University Press, doi:DOI: undefined.

Jackson, C. A.-L., and S. A. Stewart, 2017, Composition, Tectonics, and Hydrocarbon Significance of Zechstein Supergroup Salt on the United Kingdom and Norwegian Continental Shelves: A Review: Permo-Triassic Salt Provinces of Europe, North Africa and the Atlantic Margins, p. 175–201, doi:10.1016/B978-0-12-809417-4.00009-4.

Jones, I. F., and I. Davison, 2014, Seismic imaging in and around salt bodies: Interpretation, v. 2, no. 4, p. SL1–SL20, doi:10.1190/INT-2014-0033.1.

Mannie, A. S., C. A.-L. Jackson, and G. J. Hampson, 2014, Shallow-marine reservoir development in extensional diapir-collapse minibasins: An integrated subsurface case study from the Upper Jurassic of the Cod terrace, Norwegian North Sea: AAPG Bulletin, v. 98, no. 10, p. 2019–2055, doi:10.1306/03201413161.

Patruno, S., W. Reid, C. A.-L. Jackson, and C. Davies, 2018, New insights into the unexploited reservoir potential of the Mid North Sea High (UKCS quadrants 35–38 and 41–43): a newly described intra-Zechstein sulphate–carbonate platform complex: Geological Society, London, Petroleum Geology Conference series, v. 8, no. 1, p. 87, doi:10.1144/PGC8.9.

Peel, F. J., C. Travis, and J. Hossack, 1996, Genetic structural provinces and salt tectonics of the Cenozoic offshore US Gulf of Mexico: A preliminary analysis: AAPG Memoir, no. 65, p. 153–175.

Penge, J., B. Taylor, J. A. Huckerby, and J. W. Munns, 1993, Extension and salt tectonics in the East Central Graben: Geological Society, London, Petroleum Geology Conference series, v. 4, no. 1, p. 1197 LP – 1209, doi:10.1144/0041197.

Pichel, L. M., F. Peel, C. A.-L. Jackson, and M. Huuse, 2018, Geometry and kinematics of salt-detached ramp syncline basins: Journal of Structural Geology, v. 115, p. 208–230, doi:https://doi.org/10.1016/j.jsg.2018.07.016.

Quirk, D. G., N. Schødt, B. Lassen, S. J. Ings, D. Hsu, K. K. Hirsch, and C. Von Nicolai, 2012, Salt tectonics on passive margins: examples from Santos, Campos and Kwanza basins:

Geological Society, London, Special Publications, v. 363, no. 1, p. 207–244, doi:10.1144/sp363.10.

Rodriguez, C. R., A.-L. Jackson, A. Rotevatn, R. E. Bell, and M. Francis, 2018, Dual tectonic-climatic controls on salt giant deposition in the Santos Basin: Brazil GEOSPHERE |, v. 14, no. 1, doi:10.1130/GES01434.1.

Rowan, M. G., and P. Weimer, 1998, Salt-sediment interaction, northern Green Canyon and Ewing Bank (offshore Louisiana), northern Gulf of Mexico: AAPG Bulletin, v. 82, no. 5B, p. 1055–1082.

Smith, R. I., N. Hodgson, and M. Fulton, 1993, Salt control on Triassic reservoir distribution, UKCS Central North Sea: Geological Society, London, Petroleum Geology Conference series, v. 4, no. 1, p. 547 LP – 557, doi:10.1144/0040547.

Talbot, C. J., and M. P. A. Jackson, 1987, SALT TECTONICS.: Scientific American, v. 257, no. 2, p. 70–79, doi:10.1038/scientificamerican0887-70.

Taylor, J. C. M., 1998, Upper Permian—Zechstein: Wiley Online Books, p. 174–211, doi:https://doi.org/10.1002/9781444313413.ch6.

Tucker, M. E., 1991, Sequence stratigraphy of carbonate-evaporite basins: models and application to the Upper Permian (Zechstein) of northeast England and adjoining North Sea: Journal of the Geological Society, v. 148, no. 6, p. 1019 LP – 1036, doi:10.1144/gsjgs.148.6.1019.

Ulrich, M. R., J. R. Kyle, and P. E. Price, 1984, Metallic sulfide deposits in the Winnfield salt dome, Louisiana: evidence for episodic introduction of metalliferous brines during cap rock formation.: GCAGS Transactions, p. 435–422, doi:10.1306/ad4618b3-16f7-11d7-8645000102c1865d.

Volozh, Y., C. Talbot, and A. Ismail-Zadeh, 2003, Salt structures and hydrocarbons in the Pricaspian basin: American Association of Petroleum Geologists Bulletin, v. 87, no. 2, p. 313–334, doi:10.1306/09060200896.

Warren, J. K., 2006, Evaporites: Sediments, resources and hydrocarbons: 1–1035 p., doi:10.1007/3-540-32344-9.

Ziegler, P. A., 1975, Geologic Evolution of North Sea and Its Tectonic Framework1: AAPG Bulletin, v. 59, no. 7, p. 1073–1097, doi:10.1306/83D91F2E-16C7-11D7-8645000102C1865D.

Figure Captions

Figure 1: (A) Map showing the different depositional zones of the Zechstein Supergroup within the Central North Sea, as described by Clark et al., 1998. Highlighted are the 3D seismic surveys available for Clark et al., 1998 study and this study (zoomed area). Notice the dataset is located outside of the zone of syn-depositional salt flow as described by Clark et al., 1998. (B) Schematic cross-section describing an idealized deposition sequence of the Zechstein Supergroup through X-X' in A. (C) Cross-section through the one intra-Zechstein minibasin which was described in 3D by Clark et al. (1998). (D) Thickness maps of the sequences described in C are evidence for syn-depositional salt flow in the Zechstein Supergroup (Modified from Clark et al. (1998)).

Figure 2: Well correlation panel through 5 of the 6 available wells flattened on Top Zechstein (for location see Figure 1A). Wells 28/4a-2 & 28/5-1 had penetrated and logged the entirety of the Zechstein Supergroup whereas the other four had logged only the upper portion of the Zechstein Supergroup. The former two wells prove a 30-50 m thick carbonate layers at the base of the otherwise evaporite-rich sequence. All wells show the presence of anhydrite and/or layered sequences of sedimentary facies at the top of the Zechstein Supergroup.

Figure 3: (A) Base-ZSG structural map. A significant convex-to-basin shape is probably associated by the location relative to the Devil's Hole Horst (see Figure 1A for location). (B) Structural map of the top Zechstein Supergroup. Same curvilinear convex-to-basin is present, demonstrated by the salt walls architecture. (C) Thickness map of the intra-Zechstein minibasins, overlayed on a grey-scale Top Zechstein structural map. (D) location of the intra-Zechstein (in Yellow) overlayed on the structural map of the Top Zechstein structural map. (E) Top Triassic structural map not showing any clear indication for the curvilinear structures.

Figure 4: A) Location of the various salt walls (SW) and minibasins (MB) overlain on the top - Zechstein Super*g*roup structural map for orientation. B) Red circles indicate isolated salt stocks located within MB2 and beyond SW3, with few are located within SW3.

Figure 5: NW-SE trending seismic (above) and Geoseismic (below) profiles through the southern part of the dataset. Visible is the carbonate dominated margin of the Devil's Horst Hole (SW1). At the centre of the figure, a large Triassic minibasin caused the rotation of the intra-Zechstein minibasin. For location see Figure 3D.

Figure 6: Seismic cross section along the centre of MB2. Isolated salt stocks are trapped within the curvilinear minibasin. Intra-Zechstein reflection are also highlighted. For location see Figure 4B.

Figure 7: W-E trending seismic (A) and Geoseismic (B) profiles through a carbonate-halite dominated intra-Zechstein minibasins. For location see Figure 3D. (C) Map of the top carbonate-rich interval at the base of the Zechstein Supergroup. (D) N-S trending seismic (above) and Geoseismic (below) profile through the carbonate-rich base-Zechstein buildups (for location see Figure 7C).

Figure 8: W-E trending seismic (above) and Geoseismic (below) profiles through the anhydrite-halite dominated intra-Zechstein minibasins. For location see Figure 3D.

Figure 9: W-E trending seismic (above) and Geoseismic (below) profiles through SW3 showing two symmetrical minibasins in its centre. For location see Figure 3D.

Figure 10: A revised depositional model for the Zechstein Super*g*roup along the eastern flank of Devil's Hole Horst showing the different phases of syn-depositional salt flow.

Figures

Figure 1

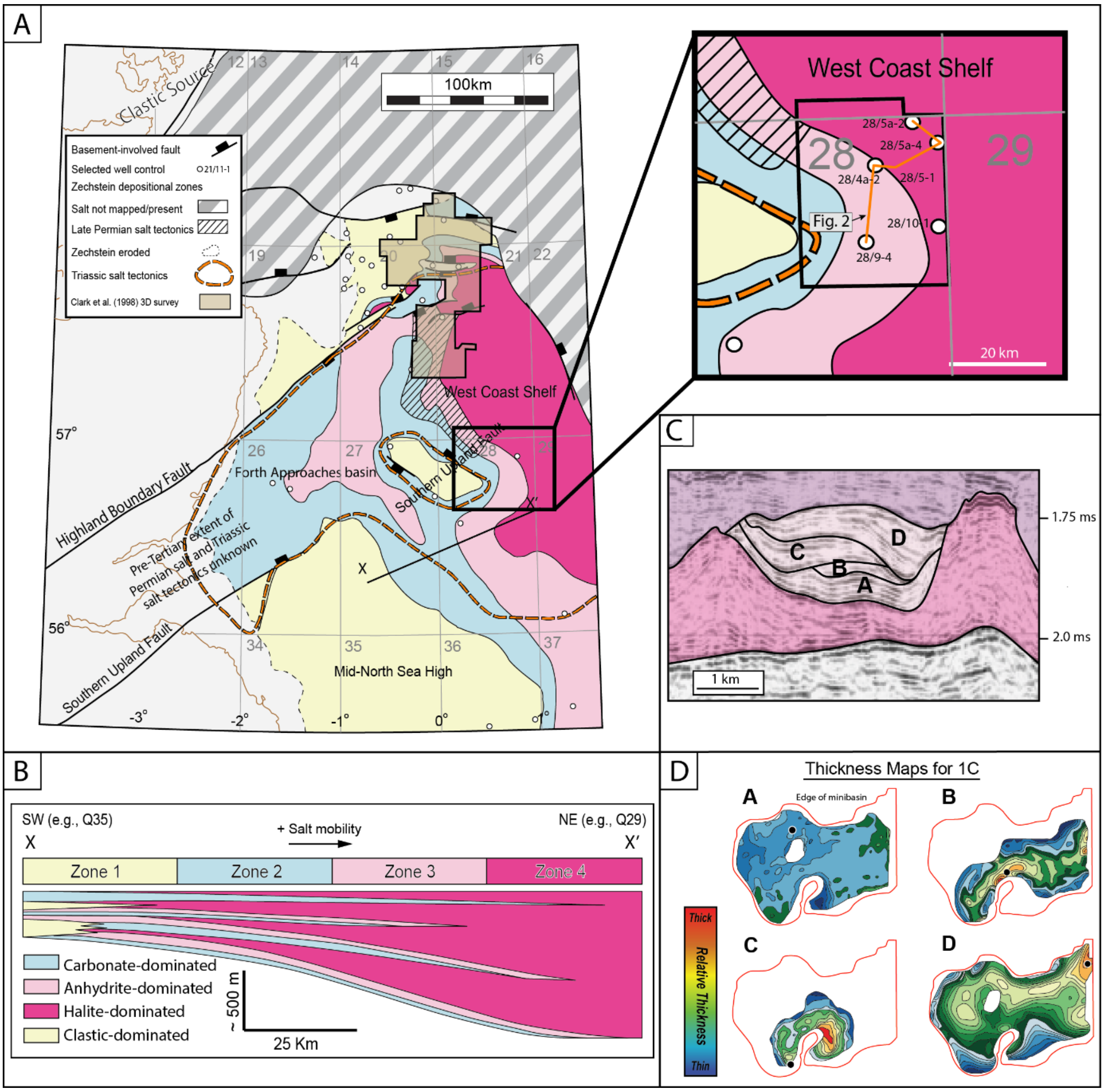

Figure 2

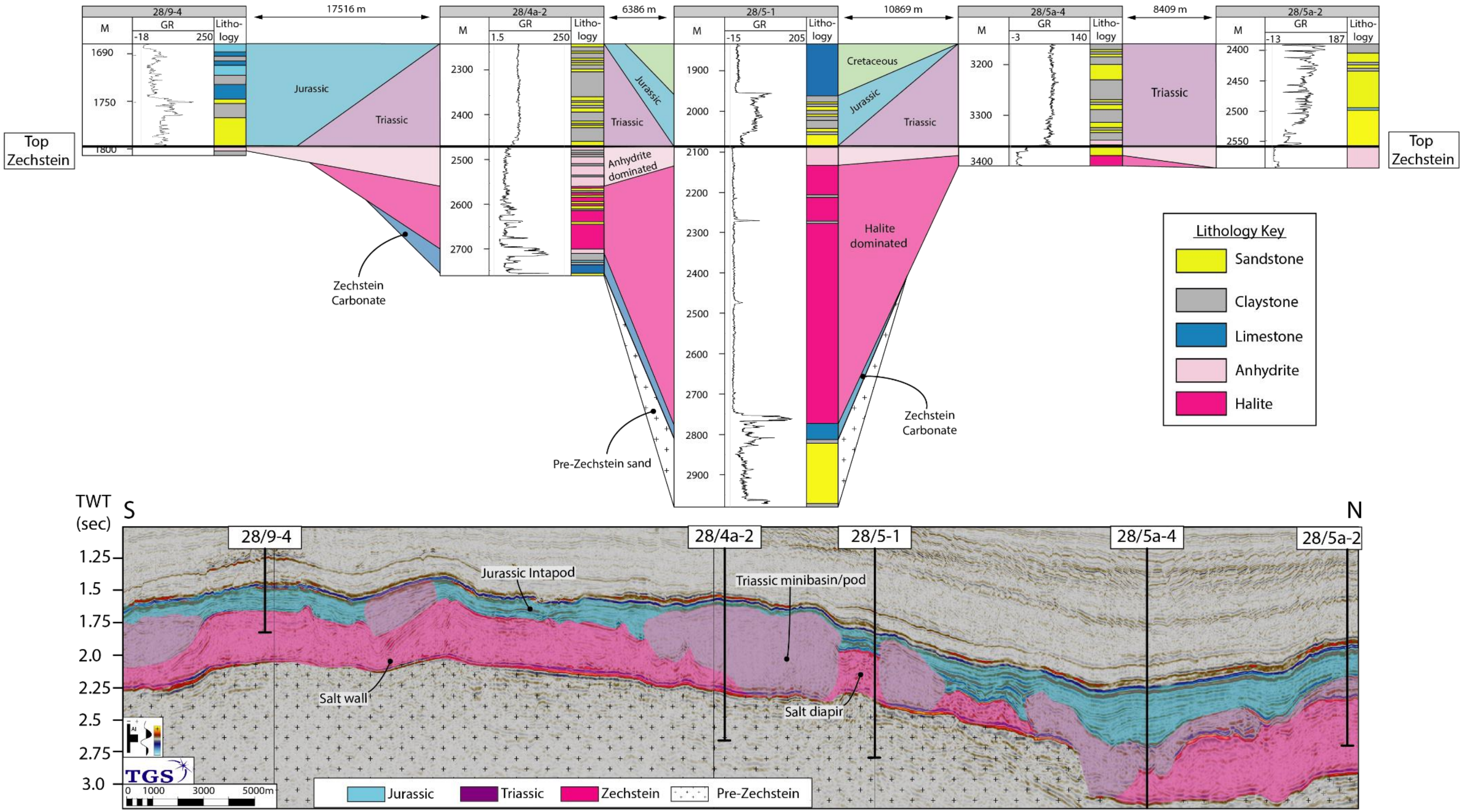

28/9-4
28/4a-2
28/5-1
28/5a-4
28/5a-2
17516 m
6386 m
10869 m
8409 m
M
GR
Litho-logy
Top Zechstein
Jurassic
Triassic
Cretaceous
Anhydrite dominated
Halite dominated
Zechstein Carbonate
Pre-Zechstein sand
Lithology Key
Sandstone
Claystone
Limestone
Anhydrite
Halite
TWT (sec)
S
N
1.25
1.5
1.75
2.0
2.25
2.5
2.75
3.0
Jurassic Intapod
Triassic minibasin/pod
Salt wall
Salt diapir
TGS
0 1000 3000 5000m
Jurassic
Triassic
Zechstein
Pre-Zechstein

585 Figure 3

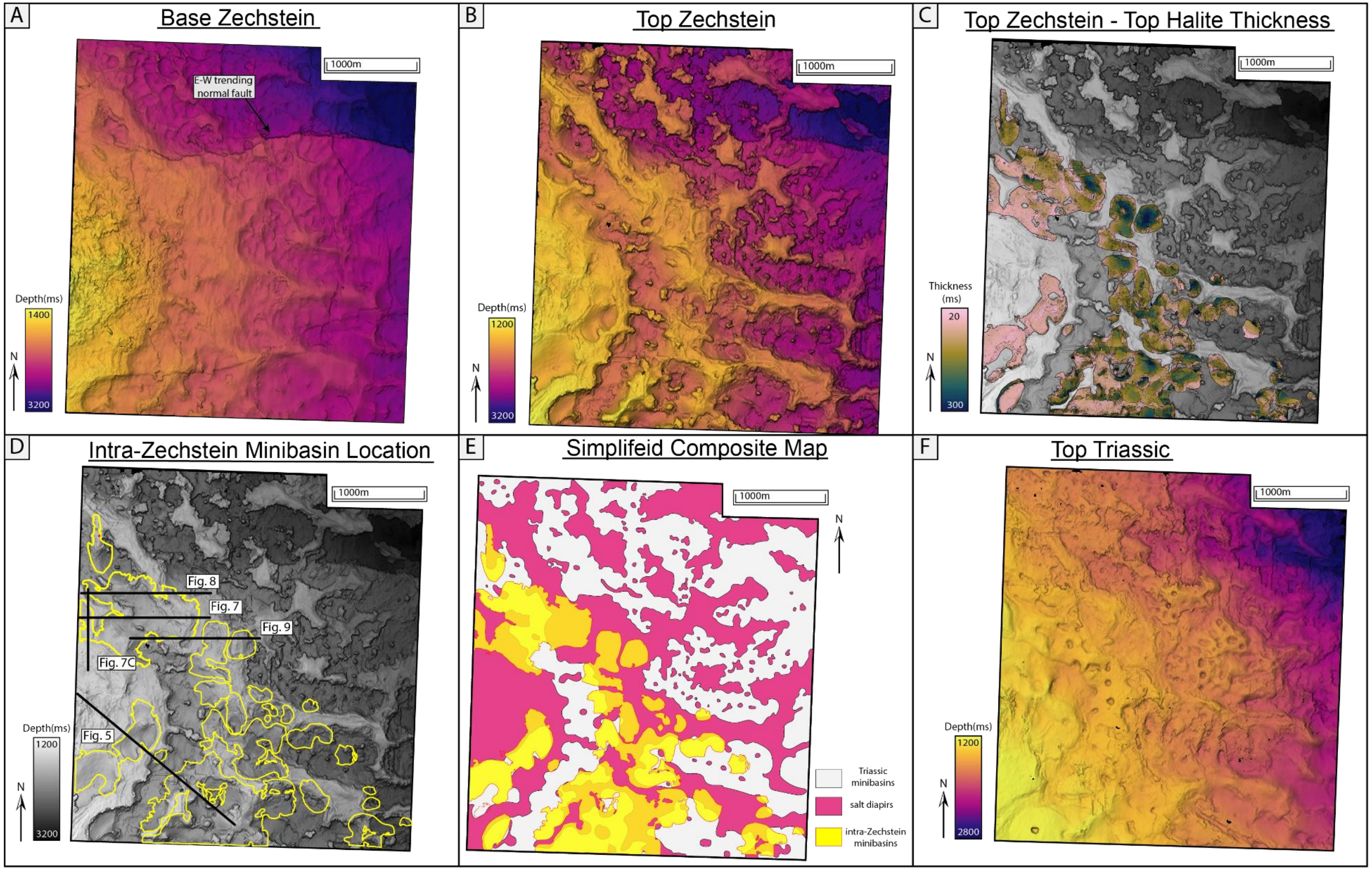

586

587 Figure 4

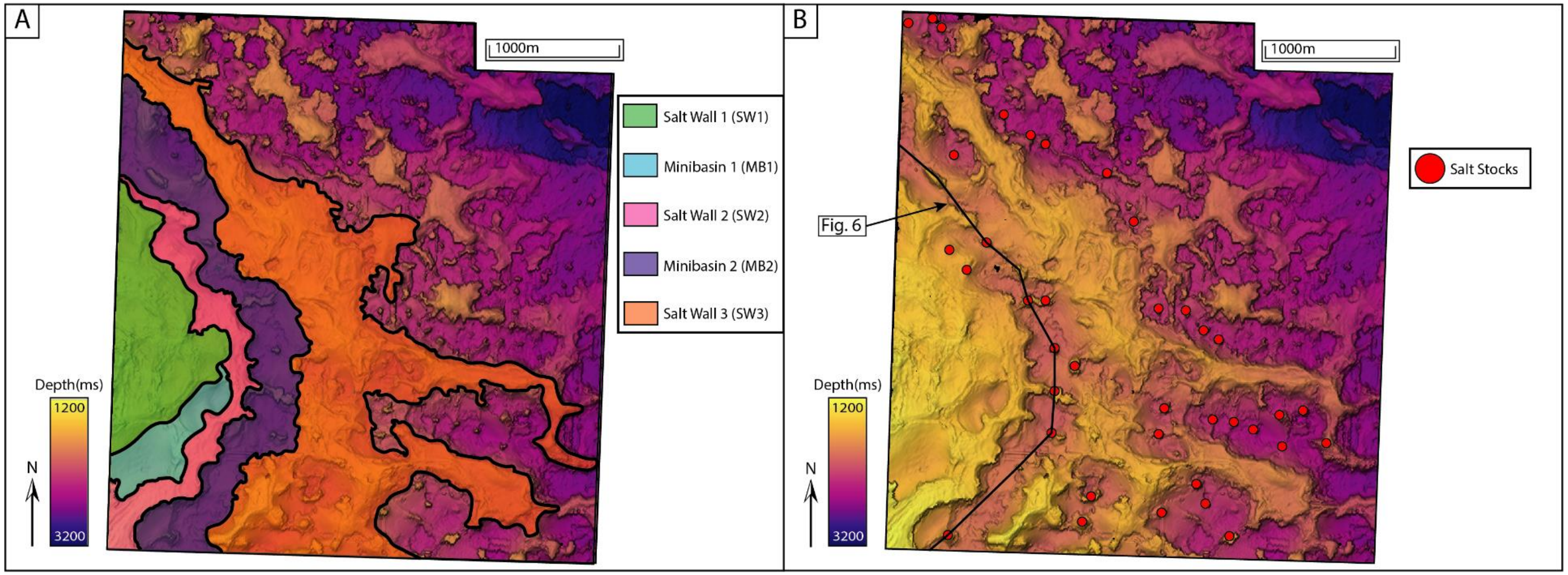

588

Figure 5

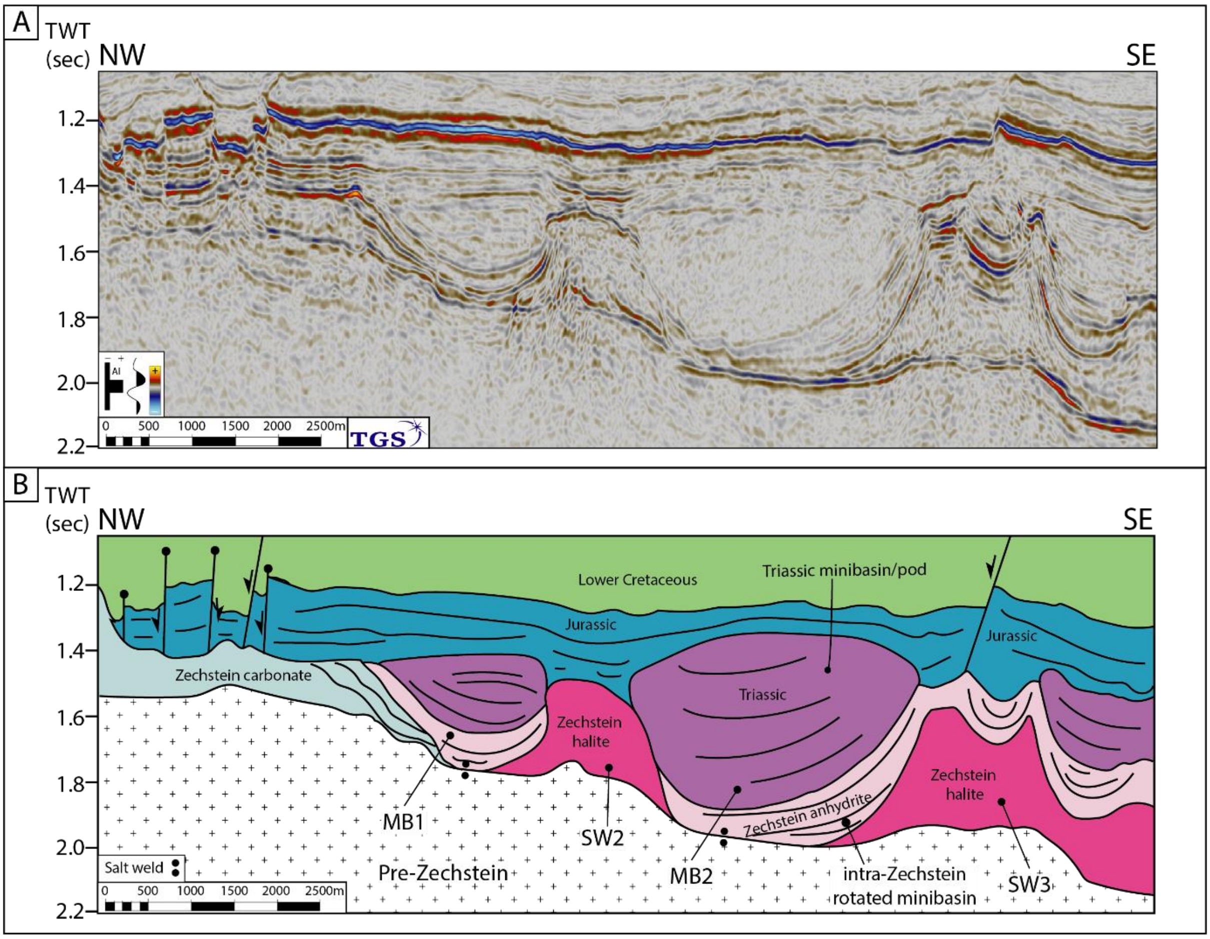
A
TWT (sec)
NW
SE
1.2
1.4
1.6
1.8
2.0
2.2
AI
0
500
1000
1500
2000
2500m
TGS
B
TWT (sec)
NW
SE
Lower Cretaceous
Triassic minibasin/pod
Jurassic
Jurassic
Zechstein carbonate
Triassic
Zechstein halite
Zechstein halite
Zechstein anhydrite
MB1
SW2
MB2
intra-Zechstein rotated minibasin
SW3
Pre-Zechstein
Salt weld
0
500
1000
1500
2000
2500m
1.2
1.4
1.6
1.8
2.0
2.2

Figure 6

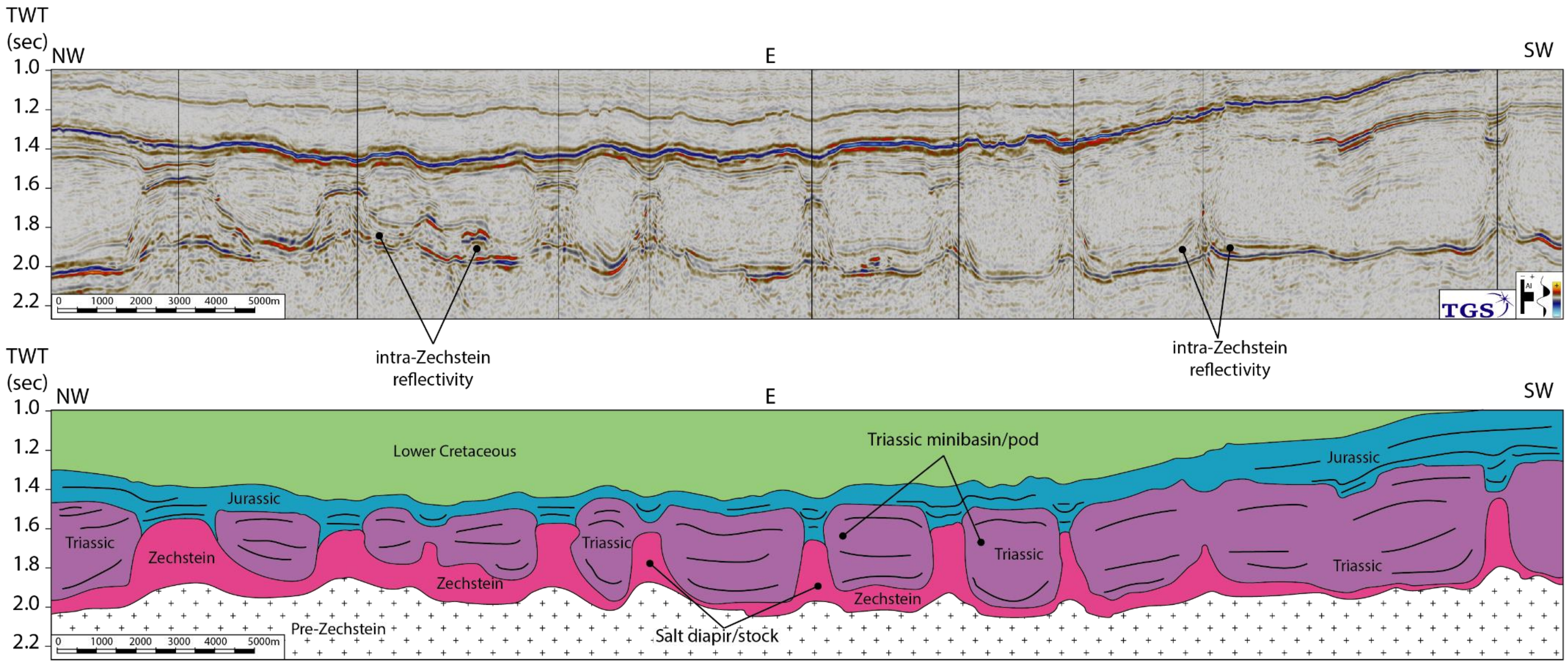

TWT (sec)
NW
E
SW
1.0
1.2
1.4
1.6
1.8
2.0
2.2
0 1000 2000 3000 4000 5000m
TGS
intra-Zechstein reflectivity
intra-Zechstein reflectivity
TWT (sec)
NW
E
SW
1.0
1.2
1.4
1.6
1.8
2.0
2.2
0 1000 2000 3000 4000 5000m
Lower Cretaceous
Jurassic
Triassic minibasin/pod
Jurassic
Triassic
Zechstein
Zechstein
Triassic
Triassic
Triassic
Zechstein
Pre-Zechstein
Salt diapir/stock

594 Figure 7

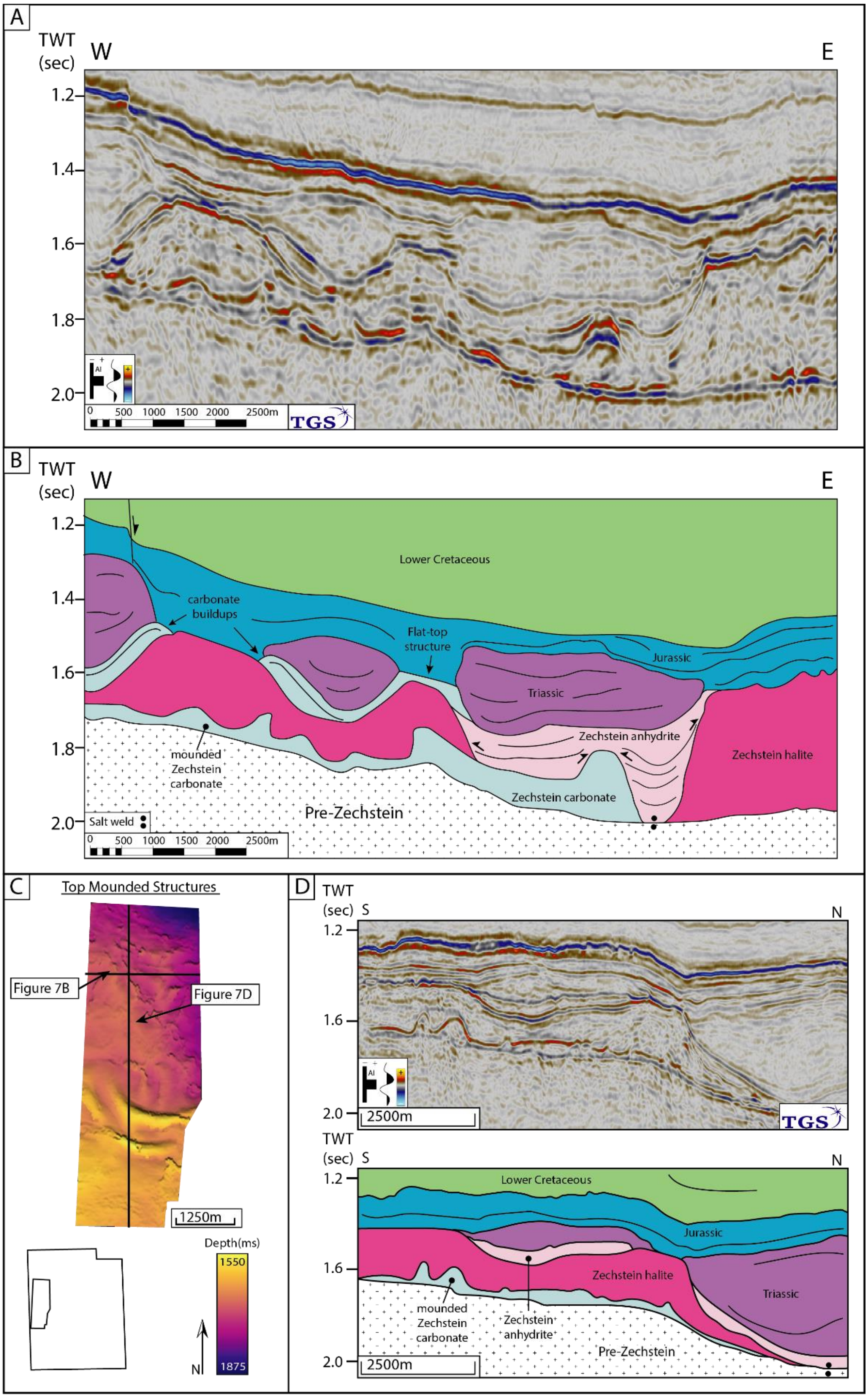

595

596 Figure 8

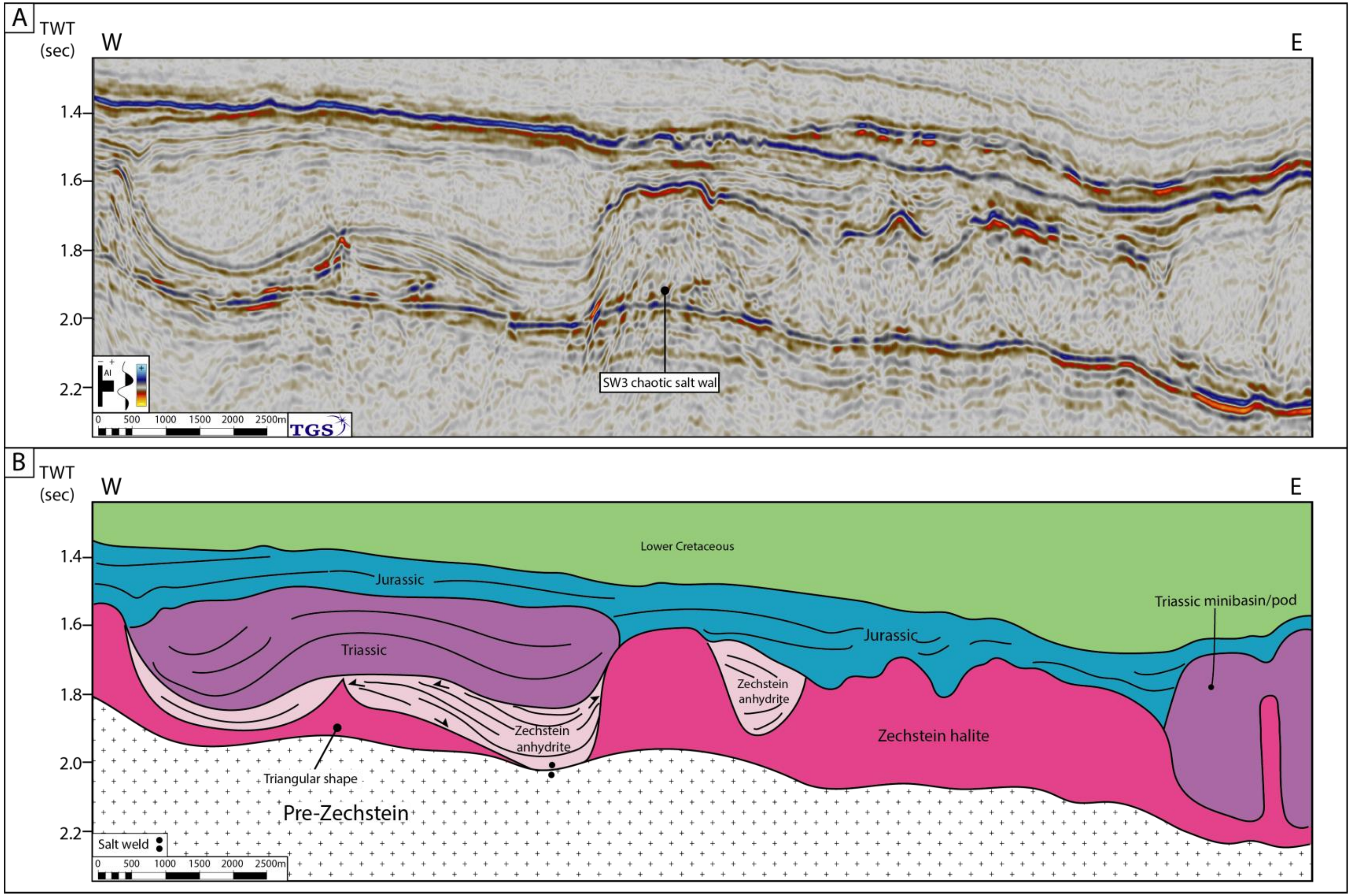

597

598 Figure 9

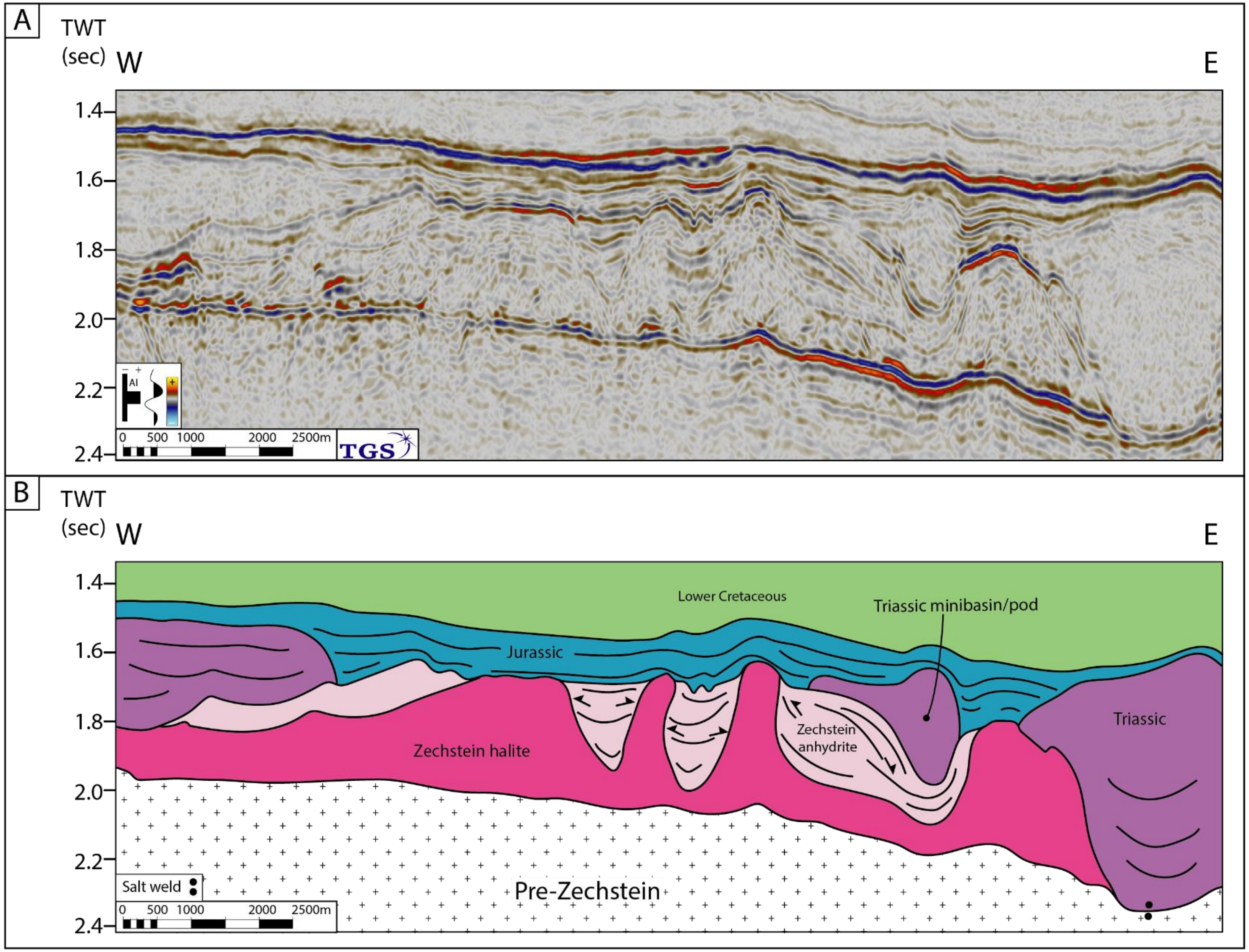

A
TWT
(sec)
W
E
1.4
1.6
1.8
2.0
2.2
2.4
AI
0 500 1000 2000 2500m
TGS
B
TWT
(sec)
W
E
Lower Cretaceous
Triassic minibasin/pod
Jurassic
Triassic
Zechstein anhydrite
Zechstein halite
Salt weld
Pre-Zechstein
0 500 1000 2000 2500m

599 Figure 10

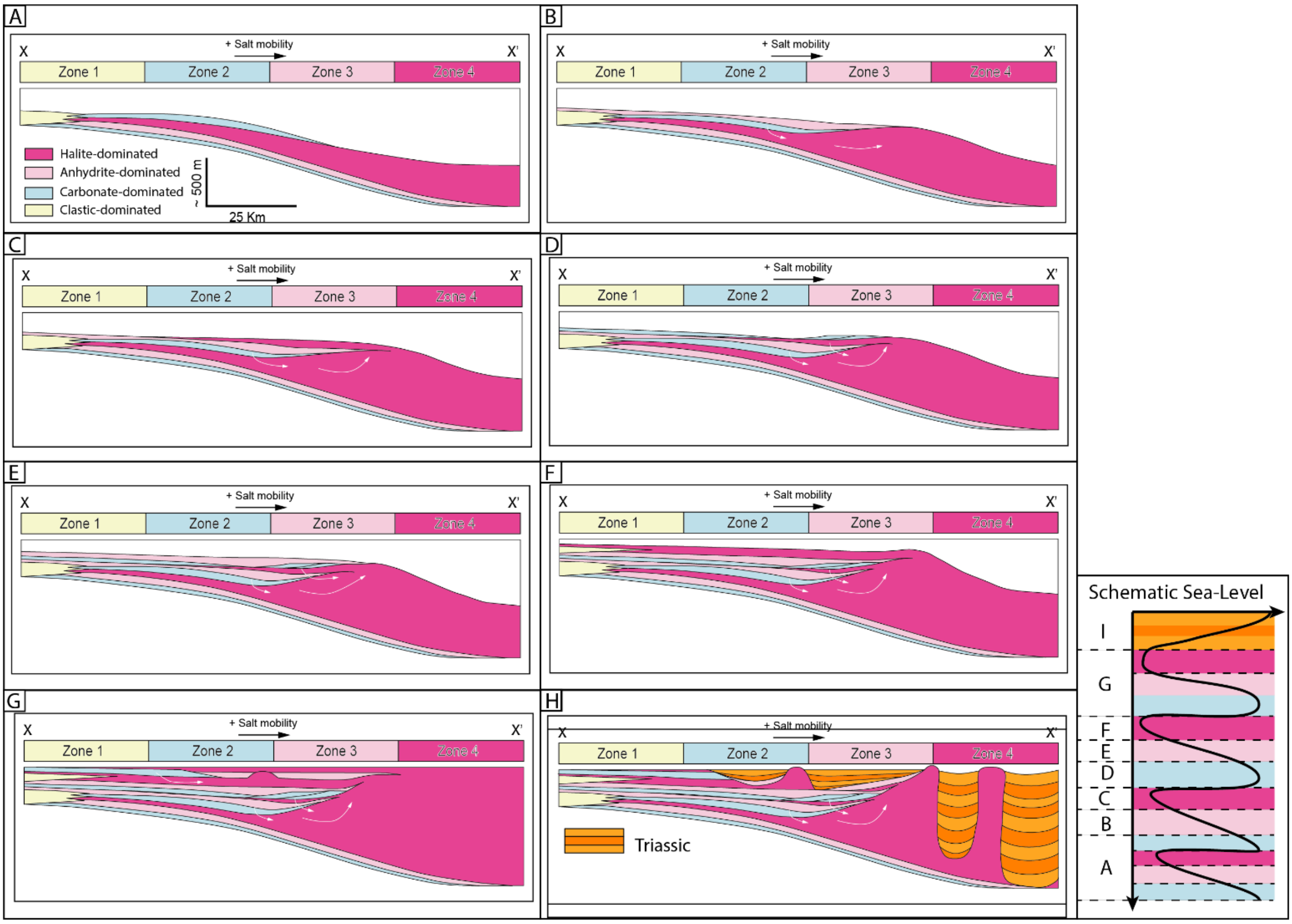

600